3

Energy Harvesters

3.1 Introduction

The energy harvester is the key component of an energy harvesting wireless communications system. Firstly, the harvester is the interface between the energy source in the natural environment and the circuit in the communications device. Thus, its design has a significant impact on the performance of the communications device. Any changes in the natural environment could be passed on to the communications device via the harvester. Secondly, the harvester supplies energy to the wireless device. Hence, the design of the wireless device also relies heavily on the characteristics of the energy harvester for efficient operation. For example, data transmission is only possible when enough energy is harvested. This necessitates the study of the conversion efficiency of the energy harvester.

In the previous chapter, we discussed some commonly used energy sources in energy harvesting wireless communications. These different energy sources will require different energy harvesters. These energy harvesters serve as transducers to convert non-electrical energy into electricity.

In this chapter, we will first discuss the principles and efficiencies of different energy harvesters. We will focus on two main harvesters that have been widely used in energy harvesting wireless communications systems: the radio frequency (RF) energy harvester and the photovoltaic (PV) panel, which convert the RF power and solar/light power into electricity, respectively.

Following the discussion of these two energy harvesters, we will examine the overall models that include both energy source and energy harvester. These models give a direct prediction of the amount and the arrival of energy available for communications without the need for any separate energy source models and energy harvester models. They have different complexity and accuracy, and thus they are suitable for different applications.

Finally, the battery and supercapacitor used as energy storage for some energy harvesting wireless communications systems will be discussed.

3.2 Photovoltaic Panels

Solar/light power is perhaps the most commonly used energy source. It can provide power for most wireless systems operating either outdoors, indoors with windows or in rooms with artificial light sources. In recent years, more and more solar-powered

Energy Harvesting Communications: Principles and Theories, First Edition. Yunfei Chen.

devices have been developed in our daily life, such as traffic display boards, sensor nodes, and roof panels. The solar power density at the outer layer of the Earth is around 137 mW/cm^2, which is available for satellites and other outer space communications devices. However, as the sunlight passes through the atmosphere, attenuation is incurred such that devices operating on the surface of the Earth can only expect a density of around 100 mW/cm^2. On cloudy days, this can be further reduced to 10 mW/cm^2. However, even for rooms with windows, a power density of around 0.5 mW/cm^2 is possible.

The efficiency of the PV cell normally ranges from 5 to 20%. This means that there is an energy loss of about 80–95%. In this case, if it is a sunny day, only 5–20 mW will be available for communications when using a PV cell with an area of 1 cm^2. The loss mainly comes from two sources: intrinsic loss; and extrinsic loss. The intrinsic loss includes photons in the solar radiation that are not absorbed by the PV cell due to energies lower than the band gap or photons that are lost to the lattice of the PV cell as heat. The extrinsic loss includes electrical loss, such as surface recombination, series resistance and shunt resistance, and optical loss, such as shading, incomplete absorption and surface reflection (Beeby and White 2010). In some cases, if the PV cell is encapsulated as a module, further loss may have incurred. All these losses add up to 80–95% of the incident light power. Thus, mathematically, the efficiency of the PV cell can be defined as

$$\eta = \frac{P}{P_i} = \frac{VI}{P_i} \tag{3.1}$$

where P_i is the incident light power at the input of the PV cell, for example, $P_i = 100$ mW on a sunny day with an area of 1 cm^2, P is the electrical power at the output of the PV cell and $P = VI$ (where V is the output voltage and I is the output current). For most PV cell studies, the relationship between V and I or the relationship between P and V are of interest, as the value of P_i depends on the operating environment only. Next, we will discuss the relationship between V and I or the relationship between P and V.

3.2.1 Principles

There are many different types of PV cells using different materials and properties. A typical silicon PV cell consists of a PN junction formed in a wafer of silicon, whose top and bottom are covered by metals to extract power from the PV cell. The upper metal contact is usually made of several separate metal fingers to allow the sun/light to arrive at the cell, while the lower metal contact is usually a continuous layer of metal. Also, the upper layer is often coated with some thin-film anti-reflective material or micro-scale texturing to minimize the optical loss due to surface reflection. Figure 3.1 shows a diagram of a typical PV cell and its components.

The principle of a PV cell is based on photoconductivity. When a photon from the light is absorbed by a semiconductor, if its energy is higher than the band gap energy of that semiconductor, an electron in the valence band will be excited into the conduction band to form an extra electron–hole pair. In this case, the conductivity of the semiconductor can be increased but after a very short period of time, the excited electron will lose its energy and recombine with a hole so that no useful electricity can be generated.

The idea of a PV cell is to physically separate electrons in the conduction band from holes in the valence band before they recombine. Specifically, a PN junction is formed by

Figure 3.1 Diagram of a typical PV cell.

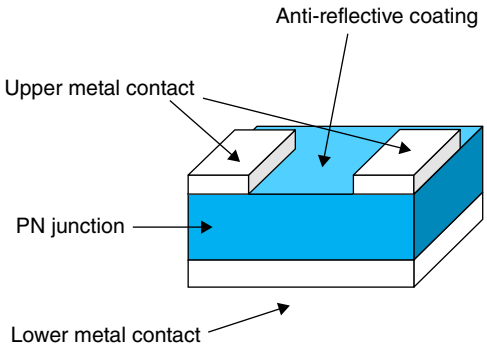

pushing a P-type semiconductor and a N-type semiconductor with different impurities together. The P-type semiconductor will gather a lot of holes, while the N-type semiconductor will gather a lot of electrons. This generates an electrostatic field and a built-in voltage across the junction. When photons fall on the PN junction, a net current will flow between P and N or a useful voltage will be generated. When a load is connected to them, power can be extracted from this current or voltage. Effectively, the PV cell is an unbiased diode, while the arrival of photons generates a photon current that adds to the drift current of this diode. Based on this equivalence, the relationship between V and I, or the $I - V$ curve can be expressed as

$$I = I_{ph} - I_0(e^{\frac{qV}{kT}} - 1) \tag{3.2}$$

where I is the output current of the PV cell, I_{ph} is the photo current generated by the incident light, I_0 is the reverse saturated current of the diode, q is the charge of an electron, k is the Boltzmann constant, T is the operating temperature of the PV cell in Kelvin, and V is the output voltage. In (3.2), the ideal diode equation has been used. Thus, a solar panel can be represented by a photon current generator connected to a diode. A diagram of such an ideal solar panel is shown in Figure 3.2.

Using (3.2), since $P = VI$, the $P - V$ curve can be derived as

$$P = [I_{ph} - I_0(e^{\frac{qV}{kT}} - 1)]V \tag{3.3}$$

Figure 3.2 Comparison of three one-diode models.

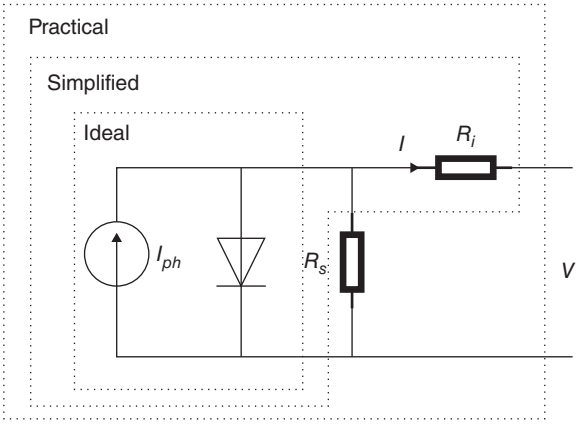

and the $P-I$ curve can be derived as

$$P = \frac{kTI}{q} \ln\left(1 + \frac{I_{ph} - I}{I_0}\right). \tag{3.4}$$

One sees from (3.4) that the output power P increases with I but decreases with $I_{ph} - I$. Hence, an optimal output power may exist. The optimal value of I that maximizes the output power is determined by

$$\ln\left(1 + \frac{I_{ph} - I}{I_0}\right) = \frac{I}{I_0 + I_{ph} - I}. \tag{3.5}$$

Using (3.3) and (3.4), the efficiency of the PV cell is calculated from (3.1) as

$$\eta = \frac{\left[I_{ph} - I_0\left(e^{\frac{qV}{kT}} - 1\right)\right]V}{P_i} = \frac{\frac{kTI}{q}\ln\left(1 + \frac{I_{ph}-I}{I_0}\right)}{P_i}. \tag{3.6}$$

Since the incident light power P_i is fixed, maximization of the efficiency is equivalent to the maximization of the output electrical power. Thus, maximum power position tracking techniques can be used to tune the parameters of the PV cell so that it can work at the output current determined by (3.5) to generate the maximum electrical power for best performance.

Note that, when the PV cell operates in the field, encapsulation may be needed to protect the cell from any damage, water, etc. It also allows the connection of multiple cells in series or parallel to increase the output voltage or the output current so that the generated output power is at a useful level. Note also that there has been a huge amount of work conducted on the device technology for PV cells. They can be categorized into first generation devices with high efficiency but high cost based on silicon wafers, second generation devices with low efficiency but low cost based on the deposit of semiconductor thin films onto inexpensive substrates such as glass or plastic, and third generation devices with even higher efficiency using multi-junctions (Beeby and White 2010). These are not discussed in detail here.

In the following, we will discuss different models of the PV cell that describe the relationship between I and V. Using them, the efficiency of the PV cell can be maximized.

3.2.2 Models

The simplest model for the PV cell is based on the ideal diode equation. It is given as (Xiao et al. 2013)

$$I = I_{ph} - I_0(e^{\frac{qV}{kAT}} - 1). \tag{3.7}$$

The only difference between (3.2) and (3.7) is that (3.7) has an additional parameter A, which is a constant called the diode ideality factor to be determined. All the other parameters are defined as before. The model in (3.7) only has three parameters to determine: I_{ph}, I_0 and A. Hence, it is the simplest model. However, this model ignores the leakage current of the diode as well as the internal resistance of the PV cell. Thus, it cannot describe the practical $I-V$ or $P-V$ curves.

To take the leakage current and the internal resistance into account, a practical model can be shown as (Villalva et al. 2009)

$$I = I_{ph} - I_0(e^{\frac{V+IR_i}{V_t A}} - 1) - \frac{V + IR_i}{R_s} \tag{3.8}$$

where R_i is the resistance in series with the diode representing the internal resistance, R_s is the shunt resistance in parallel with the diode representing the leakage current, $V_t = \frac{kT}{q}$ is the thermal voltage, and all other symbols are defined as before. This model has two extra parameters to determine: R_i and R_s. Thus, it is more complicated than (3.7). However, it takes all the important factors of a PV cell into account and hence it is more accurate.

To strike a balance between complexity and accuracy, a simplified model can also be used as (Xiao et al. 2004)

$$I = I_{ph} - I_0(e^{\frac{V+IR_i}{V_t A}} - 1) \tag{3.9}$$

where the leakage current is ignored, as it is quite small compared with the photo current and the diode current. This simplified model has one extra parameter, R_i, compared with the ideal model in (3.7), but one less parameter, R_s, compared with (3.8). Figure 3.2 compares these three one-diode models in terms of their equivalent circuits.

All the above models use one diode in their equivalent circuits. To increase the accuracy of the model further, some also proposed the use of more diodes. For example, in Babu and Gurjar (2014) and Gow and Manning (1999), two diodes were used to model the PV cell. In Nishioka et al. (2007), three diodes were used to increase the accuracy further. The larger the number of diodes used, the more accurate the model will be but the more complicated the computation will be. For this reason, existing studies hardly use any models with more than two diodes. Thus, in the following, we only discuss the two-diode models. Similar to the one-diode models, the ideal, practical and simplified two-diode models are given as

$$I = I_{ph} - I_1(e^{\frac{qV}{kA_1T}} - 1) - I_2(e^{\frac{qV}{kA_2T}} - 1), \tag{3.10}$$

$$I = I_{ph} - I_1(e^{\frac{V+IR_i}{V_t A_1}} - 1) - I_2(e^{\frac{V+IR_i}{V_t A_2}} - 1) - \frac{V + IR_i}{R_s}, \tag{3.11}$$

$$I = I_{ph} - I_1(e^{\frac{V+IR_i}{V_t A_1}} - 1) - I_2(e^{\frac{V+IR_i}{V_t A_2}} - 1) \tag{3.12}$$

respectively, where I_1 and I_2 are the reverse saturation currents of the two diodes, A_1 and A_2 are the ideality factors of the two diodes, and other symbols are defined as before. Figure 3.3 compares the three two-diode models. One sees that two extra parameters are added to each model, compared with the corresponding one-diode models. This increases the computational complexity dramatically. A comparison between these one-diode models and two-diode models can be found in Hasan and Parida (2016).

The establishment of the models in (3.7)–(3.12) is only a first step. The more important part of the modeling work is to determine the parameters of these models, as manufacturers normally do not provide the values of these parameters when the PV cells are sold. To do this, one could use experimental methods to obtain several pairs of values of V and I and then use these data to fit the curves so that the parameters of the models can be calculated. However, this method is material-specific and is required for each PV cell used. Thus, it is not efficient. On the other hand, manufacturers do provide certain data sheets for the PV cells sold. For example, all PV cell data sheets give the values of the open-circuit voltage V_{oc}, the short-circuit current I_{sc}, the voltage and the current that can achieve the maximum power V_{mp} and I_{mp}, respectively, the experimental maximum power P_{max}, the temperature coefficient for the open circuit K_v and the temperature

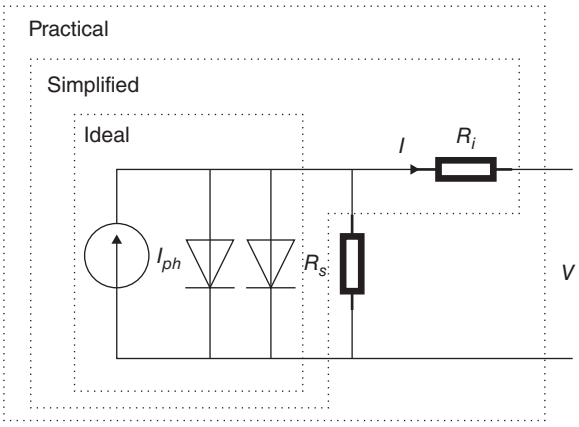

Figure 3.3 Comparison of three two-diode models.

coefficient for the short circuit K_s, under the standard testing conditions (STC) with a temperature of 300 K and a solar radiance of 1000 W/m^2. Thus, it will be useful if we can use these values to calculate the parameters of the models in (3.7)–(3.12). Next, we will use the model in (3.7) as an example to discuss this method. Note that, for some models since there are more parameters to determine than the values given in the data sheet, additional methods have to be used to obtain additional equations for the additional unknown parameters.

In the STC, when the PV cell is in short-circuit, the output voltage becomes 0. Thus,

$$I_{sc} = I_{ph}. \tag{3.13}$$

When the PV cell is in open-circuit, the output current becomes 0. Thus,

$$0 = I_{ph} - I_0(e^{\frac{qV_{oc}}{kAT_s}} - 1) \tag{3.14}$$

where T_s=300 K is the standard testing temperature. This gives the reverse saturation current as

$$I_0 = \frac{I_{sc}}{e^{\frac{qV_{oc}}{kAT_s}} - 1}. \tag{3.15}$$

Finally, the maximum power is achieved at V_{mp} and I_{mp}. This gives

$$I_{mp} = I_{ph} - I_0(e^{\frac{qV_{mp}}{kAT_s}} - 1). \tag{3.16}$$

Using (3.13)–(3.16), one has

$$\frac{e^{\frac{qV_{mp}}{kAT_s}} - 1}{e^{\frac{qV_{oc}}{kAT_s}} - 1} = \frac{I_{sc} - I_{mp}}{I_{sc}} \tag{3.17}$$

which can be solved to determine the value of the ideality factor A. Once A is obtained, it can be used in (3.16) to calculate I_0 and be used in (3.14) to calculate I_{ph}. Thus, we are able to calculate the parameters of I_{ph}, I_0 and A for the model in (3.7). In some cases, the PV cell may not operate in the STC. Thus, the parameters need to be updated according to the actual operating temperature T and radiance E. In this case, the short-circuit current can be updated to give

$$I_{ph}(T,E) = I_{sc}(T,E) = \frac{E}{E_s} I_{sc}[1 + K_s(T - T_s)] \tag{3.18}$$

where E and T are the operating radiance and temperature, respectively, E_s and T_s are the standard testing radiance and temperature, respectively, and K_s is the current temperature coefficient. Similarly, the open-circuit voltage can be updated to give

$$I_0(T,E) = \frac{I_{sc}(T,E)}{e^{\frac{qV_{oc}(T,E)}{kAT}} - 1} \tag{3.19}$$

where $V_{oc}(T,E) = V_{oc}[1 + K_v(T - T_s)][1 + K_e(E - E_s)]$ and K_e can be estimated as $K_e = \frac{(V_{0.1} - V_{oc})}{V_{oc}(1-0.8)}$. The ideality factor is determined by the material and does not change with the operating conditions. Thus, it can still be derived from (3.17). Using (3.18), (3.19), and (3.17), the model parameters in (3.7) can be determined for different temperature and solar radiance.

As mentioned before, the ideal one-diode model is the simplest model. For other models, the calculation of the parameters will be more complicated, especially for R_i and R_s. For example, curve-fitting or iteration may be required. Details of these calculations can be found in Villalva et al. (2009) and Gow and Manning (1999).

The above models describe the $I - V$ curve of the PV cell, which gives the efficiency of the energy harvester. However, due to the large variety of device technologies for PV cells, these models may not apply to all PV cells. To be more specific, they are more accurate for the silicon-based PV cells than for other PV cells. Solar/light power can provide a modest level of energy for most wireless communications systems. However, it also has two main limitations. First, it requires the device be placed in an appropriate location with as much sun/light as possible. This is to allow enough energy to be harvested. Secondly, the size of the PV cell is restricted by the applications. For example, a PV cell, used for a laptop should not be larger than the laptop, and the roof panel should not be larger than the house. This restricts the amount of energy harvested for different applications. Thus, the illumination condition, the area of the PV cell, and the overall power usage of the wireless device should be designed jointly for different applications. Next, we discuss the RF energy harvester.

3.3 Radio Frequency Energy Harvester

The RF energy harvester converts the ambient or dedicated RF power into electricity. From the hardware's point of view, it is perhaps the most suitable energy source for energy harvesting wireless communications, as most wireless systems use radio waves for information delivery too. It is even possible to use the same radio signal for both information and energy as simultaneous wireless information and power transfer. This will be discussed in Chapter 6.

Compared with batteries that require either recharging or replacement, RF energy harvesting minimizes the operational or maintenance costs. Thus, it is a useful supplemental energy source to the battery. In some harsh environments or remote places, RF energy harvesting may also be indispensable. For example, for a wireless implant in human bodies, it will be painful to replace the battery using surgeries. For wireless sensors monitoring a high-temperature turbine or nuclear reactor, it will be hard to replace the battery. It is also inconvenient to use solar power or other energy sources in these applications. Thus, RF energy harvesting has its unique advantages in wireless communications.

The amount of energy available from RF energy harvesting depends on the RF energy source. For ambient sources, such as TV signals, cellular signals and WiFi signals, as discussed in the previous chapter, the available power density is usually between 0.2 nW/cm^2 and 1 μW/cm^2. This amount is small and hence such sources are mainly used for low-power sensor networks. For dedicated sources, if near-field transfer is used, the available power density can be on the order of watts or tens of watts. This is sufficient to power up most wireless devices. On the other hand, if far-field transfer is used, the available power density varies depending on the distance. For example, with a 1 W transmitter located at a distance of 10 m, the received power could be on the order of milliwatts. The propagation environment is another important factor that affects the available energy. A suburban environment will be more friendly to RF energy harvesting than a densely urban environment.

In addition to the source and the propagation environment, the performance or the design of the energy harvester has significant impact on the harvested energy too. This can be measured by the conversion efficiency. The conversion efficiency is defined as

$$\eta = \frac{P_o}{P_i} \tag{3.20}$$

where P_i is the input power at the RF energy harvester and P_o is the output power of the RF energy harvester. For near-field power transfer, the efficiency could be larger than 80%. For ambient sources or far-field dedicated transfer, the efficiency can be between 5% and 60%. Thus, a good design is important for RF energy harvesting. In the next subsection, we will discuss the main components of the RF energy harvester. Then, we will discuss the efficiencies of RF energy harvesting.

3.3.1 Principles

The main components of the RF energy harvester include the antenna, matching network, and rectifier. Thus, in many works, it is also called a "rectenna". Figure 3.4 shows a diagram of a typical RF energy harvester. In some RF energy harvesters, there will also be a voltage regulator and a supercapacitor or battery following the rectifier. They are used for power management required by certain wireless applications. We will focus on the antenna, matching network and rectifier only.

The antenna is the first part of the harvester that captures the electromagnetic waves from the air. It is also the front end that serves as the interface between the natural environment and the energy harvester. Its efficiency is the key to the whole harvester. This efficiency depends on the frequency and the bandwidth it operates with. To increase the efficiency, multiple antennas can be used to form an array. Also, antennas operating at multiple frequencies can be used to collect as much RF energy as possible. Beamforming

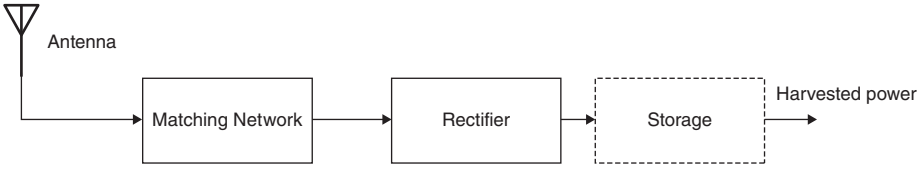

Figure 3.4 Diagram of a typical RF energy harvester.

and directional antennas can increase the efficiency further. In general, the antenna can be represented by a voltage source with a series impedance.

The overall impedance can be expressed as

$$Z_{ant} = R_{ant} + jX_{ant} \tag{3.21}$$

where the resistance R_{ant} is related to the material of the antenna as well as the antenna radiation, while X_{ant} is related to the antenna structure. For example, X_{ant} is inductive for a loop antenna and capacitive for a patch antenna. Typical values of the impedance are 300 Ω for a closed dipole antenna, 75 Ω for an open dipole antenna, and 50 Ω for other antennas.

The matching network is the second part of the harvester and lies between the antenna and the rectifier. According to the electromagnetic theories, the transmission loss is minimum or the power transfer efficiency is maximum if the impedance of the antenna equals the load connected to it. Thus, the matching network can be considered as part of the rectifier to adjust the overall impedance of the matching network and the rectifier to match that of the antenna's. This is achieved by using coils and inductors. Specifically, the matching network can be constructed using a transformer, a resistor-capacitor (RC) network or a parallel coil. Figure 3.5 shows the three different types of matching network.

In general, a RC network and a parallel coil are easier and cheaper to implement than a transformer. Thus, they are more widely used in sensor networks. Between them, a parallel coil is more commonly used for a high-impedance antenna, while a RC network is more commonly used for a low-impedance antenna.

The rectifier is the last part but the most important part of the harvester to rectify the captured alternating current into direct current for use in wireless communications. It mainly consists of diodes and capacitors. The commonly used diodes are the Schottky diodes.

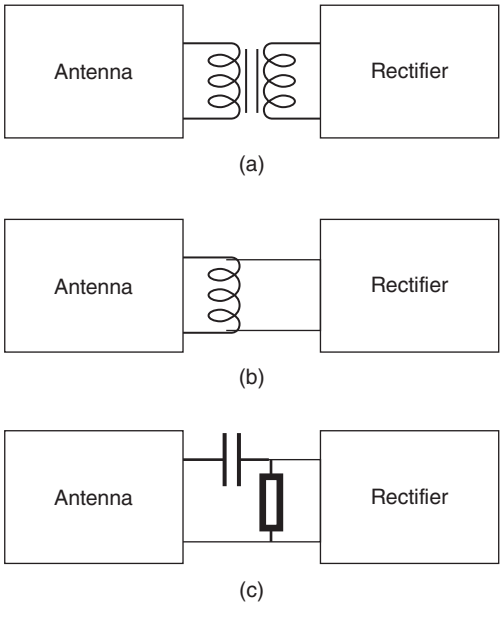

Figure 3.5 Three different matching networks: (a) transformer; (b) parallel coil; and (c) RC network.

One popular rectifier is the modified Dickson multiplier. It can rectify the RF signal and increase the output voltage for different applications. In many cases, the rectifiers are used in a number of stages to increase the output voltage or system efficiency. Each stage normally consists of two diodes and two capacitors. When the input power is low, the output voltage is relatively independent of the stage number, while the system efficiency decreases with the stage number. For a large input power, both the output voltage and the system efficiency increases with the stage number.

Both the antenna and the rectifier have efficiencies but the overall efficiency from the input of the antenna to the output of the rectifier is of more interest. Next, we examine this overall efficiency as a function of several important system parameters.

3.3.2 Efficiencies

There has been a considerable amount of work conducted on rectenna designs (Nintanavongsa et al. 2012; Stoopman et al. 2013). To compare these designs, the conversion efficiency of the RF energy harvester is a key performance measure, which is defined in (3.20). Most of these studies have given the experimental values of their efficiencies.

These harvesters can be mainly classified as harvesters for low input power and harvesters for high input power.

Stoopman et al. (2013) designed a RF energy harvester with a high sensitivity of −26.3 dBm. It works at a frequency of 868 MHz with a long distance of 25 m, when the source transmits a power of 1.78 W. Its peak efficiency is 22%. Further improvements were made in Stoopman et al. (2014), where the sensitivity was increased to −27 dBm and the range was increased to 27 m. Also, the peak efficiency went up to 37%. Stoopman et al. (2014) designed a fully passive RFID tag operating at a range of 3 m. The peak efficiency is 37%. In Scorcioni et al. (2013), an energy harvester with a peak efficiency of 60% and a sensitivity of −21 dBm was achieved at 868 MHz. The efficiency is above 30% when the input power is between 0.05 mW and 1.5 mW. Such a wide range of input power is very useful. Sun et al. (2013) designed a dual-band harvester at the GSM1800 band and 3G band to harvest energy from multiple bands. Tests showed that it has a peak efficiency of 51%, and its normal operating efficiency is between 16% and 43%. In Le et al. (2008), a 906 MHz energy harvester based on a 36-stage rectifier was designed with a peak efficiency of 60% and a sensitivity of −22.5 dBm. It can operate at a distance of 42 m from a 4 W power source but the efficiency drops quickly when the input power is higher than 0.2 mW. In Kotani et al. (2009), another GSM band harvester was designed that can achieve a peak efficiency of 67.5%. Further tests also showed that this harvester could be used for a 500 MHz TV band to achieve a peak efficiency of 80%. All these designs operate at low input power and are suitable for long-range harvesting applications. Their peak efficiencies are normally achieved at an input power of less than 0.2 mW.

Masuch et al. (2012) designed a 2.4 GHz energy harvester with a peak efficiency of 22.7% achieved at 0.5 dBm and a sensitivity of −10 dBm. In Scorcioni et al. (2012a), another energy harvester at a frequency of 868 MHz was designed for RFID and remote powering applications. This design aimed to maximize the range of the input power that provides high efficiency. An efficiency higher than 40% for a dynamic range of 14 dB in the input power was obtained. This design has a peak efficiency of 60% achieved at 0.5 mW. Nintanavongsa et al. (2012) proposed a dual-rectifier energy harvester. The harvester can achieve an efficiency above 30% for up to 30 mW. It was tuned to 915 MHz but

can be modified to other frequencies too. It achieves a peak efficiency of 72% at an input of 4 mW. These harvesters normally achieve their peak efficiencies at an input power of more than 0.2 mW.

For all these harvesters, it has been shown in Chen et al. (2016b) that their efficiency or input–output relationship can be heuristically modeled as

$$P_o = \frac{p_2 P_i^2 + p_1 P_i + p_0}{q_3 P_i^3 + q_2 P_i^2 + q_1 P_i + q_0} P_i \tag{3.22}$$

where the parameters $p_0, p_1, p_2, q_0, q_1, q_2,$ and q_3 are different for different harvesters and can be determined by curve-fitting and P_i is the input power (in milliwatts). Hence, the conversion efficiency is a function of the input power. Specifically, it often increases with the input power to reach a peak and then decreases with the input power after the peak. Table 3.1 gives the values of the fitted parameters for different harvesters, where all parameters have been normalized by q_3 (Chen et al. 2016b). In addition to (3.22), there are other non-linear models proposed for RF energy harvesters. For example, in Chen et al. (2017d), another non-linear model was proposed as

$$P_o = \frac{aP_i + b}{P_i + c} - \frac{b}{c} \tag{3.23}$$

where a, b, and c are constants that can be obtained from curve-fitting. In Boshkovska et al. (2015)

$$P_o = \frac{\frac{M}{1+e^{-a(P_i-b)}} - M\Omega}{1-\Omega} \tag{3.24}$$

where $\Omega = \frac{1}{1+e^{ab}}$ and a, b, and M are constants. Figure 3.6 compares the fitted efficiencies using (3.22) and (3.23) for the experimental data in Le et al. (2008). In general, both fitted curves track the experimental data quite well, while the model in (3.22) is slightly better than that in (3.23) by using more parameters.

The above models mainly examine the relationship between the efficiency and the input power. This is useful because it allows system designers to choose the harvester for applications with different input power to achieve the maximum efficiency.

In addition to the input power, the operating frequency and the distance have large impact on the efficiency too. Sun et al. (2013) and Song et al. (2016, 2017) studied the effect of frequency on the conversion efficiency, while Le et al. (2008) studied the effect of distance on the conversion efficiency.

Table 3.1 Fitted parameters for some energy harvesters.

Reference	p_2	p_1	p_0	q_2	q_1	q_0
Stoopman et al. (2013)	1.34	5.2e−5	1.6e−6	5.5e−2	−3.18e−4	2.87e−6
Sun et al. (2013)	4.5e5	7.6e5	685	1.11e4	1.4e4	73.1
Le et al. (2008)	78.5	−2.34	1.62	2.43	−0.482	0.0658
Masuch et al. (2012)	230	−20.5	0.623	9.24	−0.77	0.0808
Scorcioni et al. (2012a)	300	−12.7	0.135	4.4	−1e−2	−1.7e−3

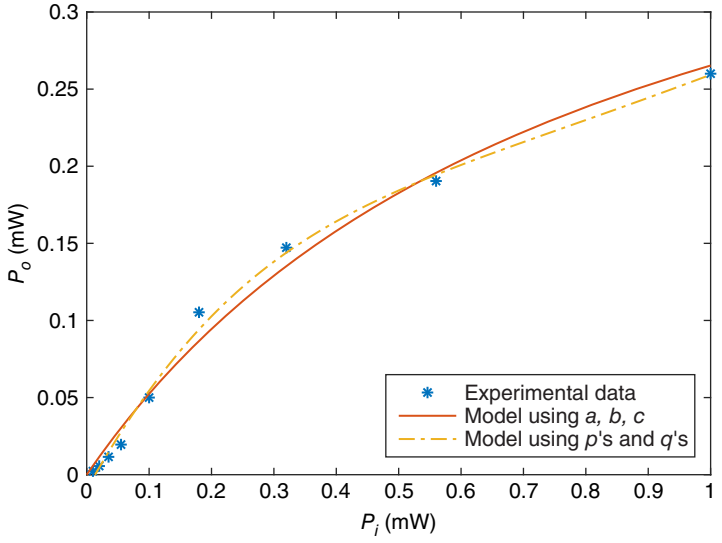

Figure 3.6 Comparison of the fitting methods in (3.22) and (3.23) with the experimental values.

For the frequency, using curve-fitting, it can be shown that the conversion efficiency is a heuristic function of the frequency following a mixture Gaussian model as

$$\eta = \sum_{i=1}^{I} a_i e^{-\frac{(f-b_i)^2}{c_i}} \tag{3.25}$$

where I is the number of Gaussian terms, f is the operating frequency, while a_i, b_i, and c_i are the parameters determined by curve-fitting. Tests show that $I = 3$ or $I = 4$ is usually enough to achieve satisfactory accuracy. The Fourier series is another good model. In this case, the conversion efficiency can be described as

$$\eta = a + \sum_{i=1}^{I} [b_i \cos(idf) + c_i \sin(idf)] \tag{3.26}$$

where a, b_i, c_i, and d are the parameters to be fitted. Figure 3.7 compares the fitted curve using the Fourier model and the experimental values in Sun et al. (2013). These models can largely track the change of the conversion efficiency caused by the frequency. They can be used to guide the choice of the operating frequency or frequencies for the RF energy harvester.

The effect of distance on the conversion efficiency can be examined in a similar way. It was found that the Gaussian mixture model and the Fourier model are applicable to the distance effect too. The polynomial model can also describe the effect of distance in some cases. In these curves, there is only one peak, where the conversion efficiency first increases and then decreases when the distance increases. Figure 3.8 compares the Fourier model with the experimental values in Le et al. (2008).

The above results have mainly focused on the PV cell and the RF energy harvester. Other energy harvesters, including piezoelectric and electrostatic harvesters that convert the mechanical energy into electricity, are also of interest. They are not discussed here.

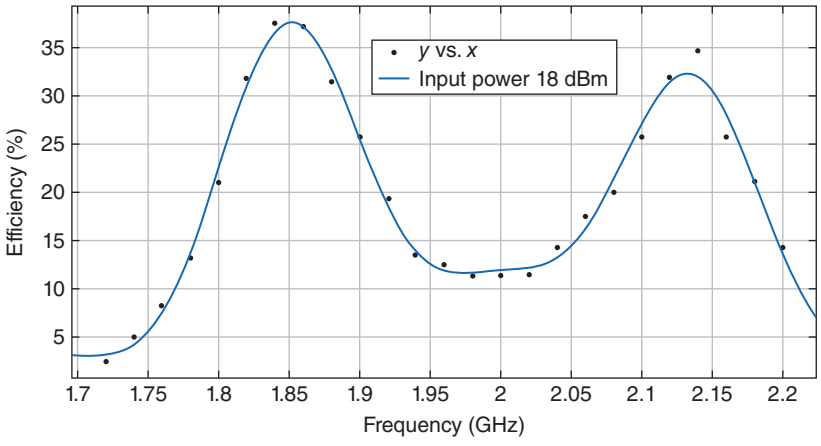

Figure 3.7 Comparison of the Fourier model and the experimental value for frequency.

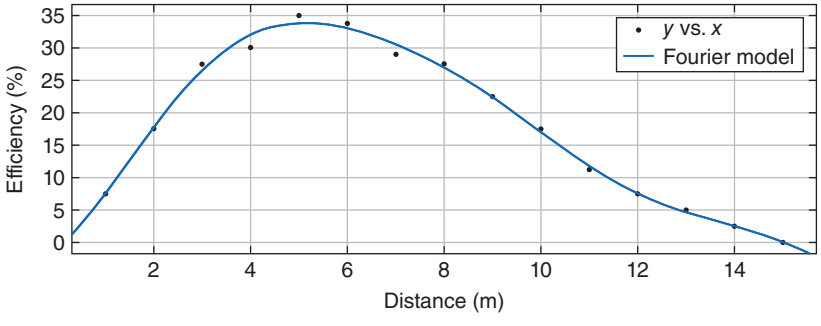

Figure 3.8 Comparison of the Fourier model and the experimental value for distance.

The models in Chapter 2 describe the change of the input power P_i. The models in the above describe the relationship between P_o and P_i. By combining them, one can model the change of the output power P_o, which is the power available for wireless communications. This can be considered as a two-step process. Alternatively, many studies have tried to model the output power P_o directly by considering the energy source and the energy harvester as a whole. In the following, we will discuss some of these modeling studies.

3.4 Overall Models

The overall model combines the energy source and the energy harvester as one whole blackbox and only models the output power of this box. There have been quite a few studies on the modeling of the harvested power.

Some of these studies used empirical methods. For example, in Lee et al. (2011), a testbed was built using the Texas Instruments eZ430-RF2500-SEH platform, which consists of a target board eZ430-RF2500T connected to a solar cell SEH-01-DK. The transmitter sends data packets in each time slot to the receiver when there is enough energy

harvested from the solar cell. Otherwise, it will stay inactive. The authors measured the number of inactive time slots between two transmissions. This is an indicator of the available energy from harvesting. The measurements were then fitted using different distributions. It was reported that the transformed Poisson distribution, the uniform distribution and the two-state Markovian model provide the best fits but there is no single distribution that has the highest accuracy in all cases. In Azmat et al. (2016), combining the measurements of the ambient RF power from the cellular bands in Chen and Oh (2016) and the RF energy harvesters designed in Kotani and Ito (2007) and Scorcioni et al. (2012b), the authors modeled the harvested RF power using different machine learning algorithms. Figure 3.9 compares the actual data and the modeled data using these harvesters at 897 and 897.2 MHz, when linear regression is applied. The model can describe the data quite well. In most cases, the prediction error is less than 15%, giving an accuracy of more than 85%.

In other studies, theoretical methods have been used. These methods can be divided into two types: deterministic models; and stochastic models. The deterministic models assume that the arrival time and the amount of the harvested energy are perfectly known. This knowledge is non-causal and hence has to be obtained offline. Using this non-causal knowledge, the transmitter can optimize its transmission strategy. However, the efficiency of the optimal transmission strategy relies heavily on the accuracy of this knowledge. Hence, they are suitable for applications where the energy sources are predictable or change very slowly, such as solar/light energy. The stochastic models do not assume any non-causal knowledge and hence can be used for online

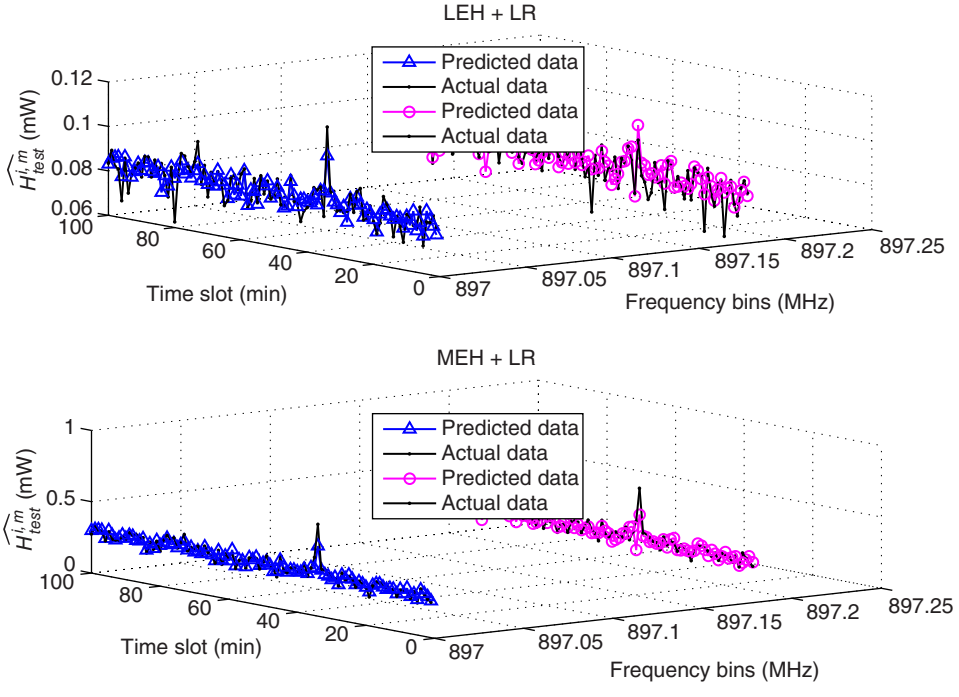

Figure 3.9 Comparison of the actual power and predicted power using linear regression (The upper part represents the results using Scorcioni's harvester and linear regression, and lower part represents the results using Kotani's harvester and linear regression.).

optimization of the transmission strategy. Instead of treating the harvested energy as a deterministic value arriving at a deterministic time, these models treat the harvested energy as a random process. They are suitable for applications where the energy source is unpredictable or random, which is the case in practice. However, there is always mismatch between the actual energy arrival and the modeled energy arrival, which may cause performance degradation.

For example, in Ozel et al. (2011), although the authors considered a Poisson counting process for the harvested energy, in the optimization, they actually assumed full knowledge of the arrival time and the amount of harvested energy at the transmitter. Hence, effectively a deterministic model was used. A similar assumption was used in Yang and Ulukus (2012) for a different optimization problem. Even if the arrival time is predictable, the amount of harvested power may still be random due to the operating environment. Hence, it would be useful to examine the effect of imperfect energy knowledge on the performances of the optimized transmission strategy in these studies.

The main focus of these modeling studies is on the stochastic model. Depending on their way of dealing with the temporal change, they can be classified as time-uncorrelated models and time-correlated models.

Examples of time-uncorrelated models include the following. In Aprem et al. (2013), a Bernoulli process is used to model the harvested energy. In this model, the time horizon is divided into equal time slots. At the beginning of the nth time slot, the harvested energy is

$$E_n = \begin{cases} E, & \text{with probability } p \\ 0, & \text{with probability } 1-p. \end{cases} \tag{3.27}$$

In addition, $E_1, E_2, \cdots, E_n$ are independent and identically distributed. Hence, this model assumes that, during each time slot, the harvester either harvests an amount of E or does not harvest any energy. This is a simple model that has been used in a number of studies. In Mao et al. (2013), a Poisson distribution is used to model the harvested energy. Again, the harvested energy arrives at the beginning of each time slot but the amount of the harvested energy follows a Poisson distribution as

$$Pr\{E_n = k\} = \frac{e^{-\lambda}\lambda^k}{k!} \tag{3.28}$$

where $k = 0, 1, \cdots$. Similarly, $E_1, E_2, \cdots, E_n$ are independent and identically distributed. This can be considered as a generalization of the Bernoulli model from a binary case to a M-ary case. There are other similar models. A common assumption made in these models is that the harvested energies in different time slots are independent. This may not be the case in practice. For example, in the ambient 3G signal, the energy is likely to be correlated within the same phone conversation across different time slots. Thus, time-correlated models may be more useful in these applications.

The most popular time-correlated stochastic model is the Markov model. In Ho and Zhang (2012), the harvested energy was assumed to follow a discrete first-order Markov process. In this case, the probability mass function of E_n is given as

$$f(E_n|E_0) = \prod_{i=1}^{n} f(E_i|E_{i-1}) \tag{3.29}$$

One sees that the harvested energy at time i only depends on the harvested energy in the previous time slot at time $i-1$. In Michelusi et al. (2013), a two-state Markov process

was used to model the harvested energy. In this case, the harvested energy is either 0 or E. One has

$$Pr\{E_n = E|E_{n-1} = E\} = p \tag{3.30a}$$

$$Pr\{E_n = 0|E_{n-1} = 0\} = q \tag{3.30b}$$

$$Pr\{E_n = 0|E_{n-1} = E\} = 1 - p \tag{3.30c}$$

$$Pr\{E_n = E|E_{n-1} = 0\} = 1 - q \tag{3.30d}$$

where $0 < p, q < 1$ are the state transition probabilities. In this model, the harvested energy changes between state E that harvests a fixed amount of energy and state 0 that does not harvest any energy. The transition either leads to a new state or keeps the current state, each with certain probabilities. Figure 3.10 shows the state transition of the two-state Markov chain model. This model has been widely used to optimize the scheduling policies in many studies. The number of states can be more than two in the generalized Markov process but the complexity increases with the number of states considered.

The empirical methods can also be combined with the theoretical methods to describe the harvested energy. For example, in Ku et al. (2015), measurements were first used to determine the mathematical models and then used to find the parameters of the models.

There are other models for the harvested energy. For example, in Flint et al. (2014), the stochastic geometry approach was used to model the harvested energy. In Chen et al. (2017d), the probability density function (PDF) and the cumulative distribution function (CDF) of the harvested RF energy from multiple antennas, multiple frequencies or multiple time slots have been derived for Nakagami-m fading signals. For example, if the harvested signals suffer from Rayleigh fading and I linear energy harvesters are used to harvest these signals for energy, the PDF and CDF of the harvested energy can be given as (Chen et al. 2017d)

$$f_{P_o}(y) = \sum_{i=1}^{I} \prod_{j=1, j\neq i}^{I} \frac{1}{2\eta_i\sigma_i^2 - 2\eta_j\sigma_j^2} e^{-\frac{y}{2\eta_i\sigma_i^2}} \tag{3.31}$$

$$F_{P_o}(y) = \sum_{i=1}^{I} \prod_{j=1, j\neq i}^{I} \frac{2\eta_i\sigma_i^2}{2\eta_i\sigma_i^2 - 2\eta_j\sigma_j^2} [1 - e^{-\frac{y}{2\eta_i\sigma_i^2}}] \tag{3.32}$$

where η_i is the conversion efficiency of the ith RF energy harvester and σ_i^2 is the average fading power of the ith signal. Details of the derivation and more cases can be found in Chen et al. (2017d). These models allow efficient designs of energy harvesting wireless communications systems. Next, we will discuss the battery or supercapacitor used in energy harvesting wireless.

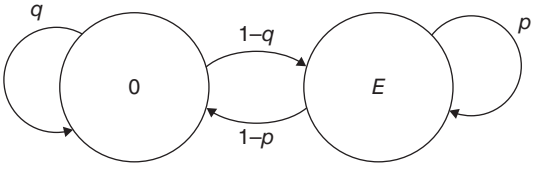

Figure 3.10 Two-state Markov chain model.

3.5 Battery and Supercapacitor

A battery or supercapacitor is not always required in an energy harvesting communications system. It depends on the protocol of energy usage in the system. For example, in the harvest-use protocol, the energy is used immediately after being harvested so that no buffer is required (Krikidis et al. 2013). In this protocol, wireless communications is performed on a best-effort basis. When there is enough energy, it will transmit data. Otherwise, it stays inactive. The quality of service (QoS) is not guaranteed in this protocol. However, in many wireless applications, QoS is important. Thus, although the energy harvester aims to replace the battery in wireless communications, in these applications, a rechargeable battery or a supercapacitor is still required to accumulate and preserve the harvested energy so that it can be saved for later use. Also, when the harvested energy is larger than the required amount, the excess energy can also be stored to reduce the effect of variation in energy source. In this section, the battery and supercapacitor will be discussed.

3.5.1 Battery

An ideal battery contains a certain amount of energy units. When the wireless device is in operation, the operation consumes a fixed amount of energy units to reduce the battery capacity. Otherwise, the capacity stays the same for any future use. In practice, all batteries suffer from leakage. Even when the battery is not in use, its capacity decreases due to internal chemical reactions. Further, the charge and discharge of the battery will not be perfect such that their efficiency will be less than 100%, implying that some energy units will be lost during the charging and discharging processes. In addition, batteries suffer from non-linear distortions. For example, the rate-dependent capacity actually decreases in a non-linear way with the discharge rate so that a higher discharge rate leads to a much lower capacity. Also, the operating temperature can affect the discharge and the leakage considerably, as it accelerates or decelerates the chemical reactions inside the battery. Finally, the maximum capacity of the battery decreases with more charges and discharges. The voltage changes as well during discharge. These characteristics will affect the battery performance and therefore affect the performance of the energy harvesting wireless system.

To examine and describe the characteristics of rechargeable batteries, many types of battery models have been proposed (Rao et al. 2003) and this is still an on-going effort. These models can be classified as physical models, empirical models, abstract models, or their combination. The physical models simulate the actual physical and chemical processes inside the battery to understand the principles underpinning an electrochemical battery (Doyle et al. 1993). They are usually very accurate but have very high computational complexity at the same time due to the many processes that affect the performance of a battery. The empirical models use measurement data to approximate the behavior of the battery with simple equations (Syracuse and Clark 1997). They have low computational complexity but low accuracy too. Also, the models vary from battery to battery so that their generality is not high. The abstract models emulate the battery behavior by using simple equivalent representations, such as stochastic systems and circuits (Bergveld et al. 1999). Their complexity and accuracy are between the physical models and the empirical models.

3.5.2 Supercapacitor

A supercapacitor is another type of energy storage commonly used in energy harvesting communications. They are capacitors with very high capacitance in a small size and are suitable for wireless communications for several reasons. Firstly, unlike batteries that can only be charged and discharged for a finite number of times (1000 cycles in many cases), supercapacitors can be charged and discharged almost for an unlimited number of times. Thus, they last longer and are more suitable for energy harvesting wireless communications that aim to minimize maintenance cost. Secondly, unlike batteries that need some protection circuits, supercapacitors only need very simple charging circuits and can be charged more quickly with higher efficiencies. Finally, they are more environmentally friendly than batteries in terms of disposal. Similar to batteries, supercapacitors also suffer from charging and discharging losses with less than 100% efficiencies, as well as leakage and changing voltage and capacity.

In general, supercapacitors have smaller capacities than rechargeable batteries due to their size limitation. Hence, leakage becomes very important for supercapacitors, as the leaked electricity could be significant compared with the energy harvested by and stored in supercapacitors. The leakage depends on several important factors, such as the capacitance, the amount of stored energy and the temperature. It is very hard to find theoretical models to describe the leakage as a function of these factors. Hence, the leakage pattern is often examined experimentally. For example, based on measurements, constant leakage current, exponential leakage voltage, polynomial approximation or piecewise linear approximation can be used (Renner et al. 2009; Zhu et al. 2009). One major disadvantage of supercapacitors is that their voltage decreases linearly to zero as the stored energy is being used so that their residual energy cannot be used in wireless communications, as most wireless nodes have a minimum voltage requirement below which they do not work.

3.6 Summary

In this chapter, we have examined the energy harvesters used for energy harvesting wireless communications. We have discussed the principles and theories for two commonly used energy harvesters: the RF energy harvester that converts RF power into electricity; and the PV cell that converts solar/light power into electricity.

The PV cell uses the photoconductivity effect to convert the incident light power into electricity. This is a well-established technique and can provide a modest level of energy that is sufficient for most energy harvesting wireless applications. The PV cells can be modeled by equivalent circuits using one or two diodes. Their input–output relationships are quite simple, although the determination of the model parameters requires considerable effort.

The RF energy harvester has unique advantages in wireless communications as many wireless communications are implemented using RF signals. It mainly consists of an antenna that captures the radio waves and a rectifier that rectifies the captured waves into direct current for use in wireless communications. The amount of energy harvested from the RF power and its conversion efficiency depend on the techniques used. Near-field harvesting can provide a harvested power of several watts with

efficiencies higher than 80%, while far-field harvesting can only provide a harvested power of several milli- or microwatts with efficiencies between 5% and 60%. The actual efficiency depends on various factors, such as the input power, the frequency and the operating distance. Their non-linear relationships have been discussed.

A supplementary component of energy harvesting wireless communications is energy storage. Both rechargeable batteries and supercapacitors have been discussed. The supercapacitors have advantages in charging efficiency, charging time and lifetime but disadvantages in leakage and residual energy, over the rechargeable batteries. Also, to understand how batteries work and how the leakage occurs, different models have been proposed.

The ultimate goal of the discussion on the energy harvester and the discussion on the energy source is to understand how the energy flows from the source to the harvester and then from the harvester to the communications device. These two processes can be combined in one study to model the energy available for communications directly. Various models have been proposed to model this energy. Among them, the two-state Markov model is widely used.

Next, we will move on from the energy harvester to the communications device to understand how the communications device can be redesigned based on the characteristics of the energy harvesting process.